

Incorporation of a time-dependent thermodynamic model and a radiation propagation model into infrared three-dimensional synthetic image generation

John R. Schott, MEMBER SPIE

Rolando Raqueño

Carl Salvaggio

Center for Imaging Science

Rochester Institute of Technology

Digital Imaging and Remote Sensing

Laboratory

Chester F. Carlson Building

Rochester, New York 14623-0887

Abstract. A model is presented for generation of synthetic images representing what an airborne or satellite thermal infrared imaging sensor would record. The scene and the atmosphere are modeled spectrally with final bandwidth determined by integration over the spectral bandwidth of the sensor (the model will function from 0.25 to 20 μm). The scene is created using a computer-aided-design package to create objects, assign attributes to facets, and assemble the scene. Object temperatures are computed using a thermodynamic model incorporating 24-h worth of meteorological history, as well as pixel specific solar load (i.e., self-shadowing is fully supported). The radiance reaching the sensor is computed using a ray tracer and atmospheric propagation models that vary with wavelength and slant range. Objects can be modeled as specular or diffuse with emissivities (reflectivities) dependent on look angle and wavelength. The resulting images mimic the phenomenology commonly observed by high-resolution thermal infrared sensors to a point where the model can be used as a research tool to evaluate the limitations in our understanding of the thermal infrared imaging process.

Subject terms: image simulation; synthetic image generation; infrared.

Optical Engineering 31(7), 1505-1516 (July 1992).

1 Introduction

Thermal infrared (TIR) imagery generated by midwave (3- to 5- μm) and longwave (8- to 14- μm) sensors is being increasingly used for a variety of remote sensing applications. Some of this interest is motivated by the temperature information encoded in these images, whereas other interest is driven by the need for high-resolution sensors with day and night capability. Whatever the motivation, the fact that the appearance of these images is controlled in part by temperature introduces a complex new variable into the image analysis process. As a result, the interpretation of these images becomes very complex, particularly if quantitative information is desired. The appearance of this imagery is a result of the complex interaction of atmospheric effects, local meteorological conditions, solar load, object temperature, object emissivity, look angle, sensor location, and sensor spectral characteristics. The temperature of an object in a scene is a complex function of its thermodynamic properties and the environment in which it is located. The end result is images that exhibit contrast reversals as a function of look angle and time of day and a myriad of other unusual phenomena that even a trained image analyst may find inexplicable.

Thermal infrared synthetic image generation (TIRSIG) offers one potential tool for dealing with this process. If the models used in the TIRSIG process are based as much as possible on first principles physical models, then the images can be analyzed both in the forward fashion to see what effect a phenomena will have on an image and in a reverse fashion to determine what caused an observed effect. This paper describes a TIRSIG model that was developed as an attempt to simulate the complex interactions taking place in the thermal infrared imaging process. It incorporates the results of research on modeling many aspects of the imaging and thermodynamic process. Its overall objective is to determine if phenomena observed in TIR images can be modeled adequately so commonly observed effects can be simulated and the modeling process then used to better analyze the image formation and image analysis process.

From a scientific standpoint, a major value of synthetic image generation is that it can provide a complete end-to-end model of the image chain. The extent to which a modeled scene matches an actual scene provides a measure of how well we understand the imaging process. Conversely, the mismatch between a modeled and an actual scene can provide clues to where our understanding of the physical or engineering principles are flawed.

This effort was aimed at building an improved thermal infrared synthetic image generation model based on physical principles. This model draws on earlier work that incor-

Paper 05091 received Sep. 9, 1991; revised manuscript received Dec. 21, 1991; accepted for publication Dec. 21, 1991.
© 1992 Society of Photo-Optical Instrumentation Engineers. 0091-3286/92/\$2.00.

porated three-dimensional wire frames, angular emissivity effects, and extensive radiation propagation models for generation of longwave infrared (LWIR) synthetic images. The new digital imaging and remote sensing (DIRS) laboratory image generation (DIRSIG) model incorporates the following improvements: (1) solar radiometry effects so that mid-wave infrared (MWIR) can be modeled, (2) a thermal model so that the temperature of each scene element is computed as part of the modeling process, (3) an enhanced ray tracer that generates a full shadow history allowing for proper computation of thermal loads, (4) an enhanced radiometry model that generates and utilizes spectrally dependent variables, and (5) an integrated computing environment. These improvements enable the DIRSIG model to simulate many more of the complex physical phenomena that affect TIR images. In particular, included are solar shadows; specular and diffuse objects; sky and object background effects; and the wavelength dependent interplay of the source, sensor, and atmosphere. In addition, the thermal model allows for inclusion of thermodynamic variables such as density, heat capacity, and absorptivity for each object facet and scene dependent treatment of environmental variables such as wind speed, relative humidity, and air temperature as a function of time. The resultant images clearly reflect these improvements by visually mimicking the phenomenology observed in actual TIR images. No quantitative evaluation of the overall model has yet been performed, however, the effects shown in the simulated images have been observed in actual imagery. In addition, most elements of the overall model have been evaluated and indicate that the model should have reasonable quantitative capabilities.

2 Literature Review

Many existent TIR scene generation models are considered corporate confidential or have classified components. As a result, the literature is often limited to general descriptions making it difficult to evaluate the true capabilities of these approaches. These same limitations often make it difficult to incorporate components of these models into next generation models. Within these constraints, DCS Corporation and Schott¹ conducted an extensive literature review of models related to TIRSIG, which included CAD/CAM, IR radiation propagation, thermodynamic-energy matter interaction, ray tracing, and IR sensor models. They described over 30 models, which include numerous submodels. In many cases, these models perform only some part of the overall TIRSIG process or are very specific to a particular set of targets or sensors. Thus, only a few comprehensive models exist or can be created by stringing these submodels together.

Most existing TIRSIG require similar types of input data. Properly simulating an object in an environment requires: (1) a geometrical representation of an object (usually computer graphics), (2) some form of an atmospheric transmission model (such as obtained² from LOWTRAN or a simplifying expression such as Beer's Law), and (3) material characteristics such as emissivity or absorptivity. Some of the more elaborate simulators also include thermodynamic models and texturing capability.

A good example of TIRSIG is described by Cathcart and Sheffer³ and Sheffer and Cathcart.⁴ (We use this work as a case study, mentioning others who have done significantly different work.) They describe a program for generating

synthetic images called Georgia Tech visible and infrared synthetic imagery testbed (GTVISIT). GTVISIT requires the outputs from other modeling programs, such as GTSIG and IRMA, which are also discussed.

GTVISIT separates scenes into two components, a gridded background and faceted objects. Backgrounds consist of terrain, ocean, sky, or a combination of the three. GTVISIT uses four gridded databases: feature (material type), elevation, radiance, and TIR reflectance. The feature and elevation data may come from real-world sources (such as satellite imagery and elevation measurements), from synthetic data, or from a hybrid combination. The radiance and TIR reflectance data are generated from the temperature and/or reflectivity of each material. Such assignments typically are obtained from measured data or thermal predictions. GTVISIT creates images by using a Z-buffer algorithm; Z-buffering is a computer graphics technique used to determine hidden surfaces and modify their display. The atmospheric attenuation and emission along the viewing path are computed. To save computation time, GTVISIT precomputes radiance values for 12 orientations of each object in the scene. Radiance values are also precomputed and assigned to each vertex of a facet. If a pixel lies inside the facet, the pixel radiance is computed by interpolation. The code can include backgrounds and diurnal variation, as well as dynamic processes such as fire, smoke, and dust clouds.

GTSIG, a separate modeling program developed by Georgia Tech, computes the thermal radiance of objects from a first-principles thermal prediction code. It employs a 3-D thermal network analyzer and a multisurface radiosity technique in the computations. The physical processes included in the thermal model are solar and sky radiation (direct and occluded); mass-transfer processes (evaporation, condensation, sublimation, and precipitation); fluid flow effects; shadowing; and multisurface reflections.

IRMA is a semiempirical, one-dimensional heat transfer approach to computing the radiance for each facet of an object based on its thermal history.⁵ An IRMA model is more easily constructed than a GTSIG model.

Radiance values determined from GTSIG are reasonably robust, but do not account for angular emissivity, which is critical⁶ in the TIR. The precomputation of radiance values is acceptable, but may not be appropriate when attempting to generate an exact radiometric image (e.g., when spectral variation within the band is important). GTSIG does not address target/background radiance interactions, however, Georgia Tech has suggested this improvement. A recent report⁷ on this model indicates that direct solar shadows are now treated, but the solar shadow history for each pixel is not included in the thermal models.

Biesel and Rohlfing⁸ describe a real-time system to simulate forward looking infrared (FLIR) imagery. Real-time scene simulation can be achieved by assuming thermal equilibrium of the object with its environment, and limiting temperature to 256 distinct values. Object warming is limited to solar radiation or diffuse sky contributions. Specular reflection is neglected and atmospheric attenuation is calculated using Beer's law approximations. This approach provides real-time simulation, but at the expense of precise radiometry.

The Night Vision and Electro-Optics Laboratory (NVEOL) [now called the CECOM Center for Night Vision and Electro-

Optics (CCNVEO)] has developed a TIR model that predicts radiation distributions of a scene.⁹ The thermal signatures are calculated via an empirical model based on actual data. A specialized atmospheric attenuation routine (LTR) was validated against LOWTRAN 6. The technique has the limitation that it relies on the artistic talents of cartoonists to create individual frames. Overlays are used to simulate background objects (e.g., mountains).

Gardner et al.¹⁰ described the use of mathematical texture functions along with simple surfaces to simulate features such as hills, trees, and clouds in the visible wavelengths. The U.S. Army Tank Automotive Command (TACOM) has extended this technique to the TIR by substituting statistical characteristics of measured data for the texture function. This approach can be used for low interest background regions for tactical applications, but generally a more complete modeling is required for detailed scene analysis.

Stets et al.¹¹ describes an approach developed for simulating aircraft with various backgrounds. Spectral infrared imaging of targets and scenes (SPIRITS) is a specialized model for particular targets. Its capabilities include production of thermal plumes from an aircraft engine's exhaust, and when combined with a background model AERIE it can simulate the influence of clouds on a target/background scene. The radiometry is calculated using SPIRITS, and LOWTRAN 6 is used for atmospheric attenuation computation. This approach has the limitation that the thermal properties of the backgrounds are not computed as part of the modeling process and it does not attempt to deal with high-resolution ground scenes.

This review pointed out the capabilities of some existent models in an effort to highlight the features that would be desirable in improved models. Several limitations were noted. First, most of the models are not spectrally dependent (i.e., the solution is not done wavelength by wavelength for all dependent variables). Second, many of the thermal models do not incorporate the thermal history of an individual pixel in terms of temporal environmental variables such as sun/shadow history, air temperature, wind speed, etc. Third, most of the models do not include emissivity values that are a function of view angle. Fourth, most of the models do not include a capability to deal with specular reflections to a sky or background whose radiance varies with angle. Finally, many of the models are not based on fundamental physical principals, making them difficult to validate, integrate, or update. For several years, with this context in mind, we have been working with and evolving certain TIRSIG tools aimed at filling gaps in the modeling process.

The DIRS laboratory at the Rochester Institute of Technology's (RIT's) Center for Imaging Science has had a long-term interest in absolute radiometric calibration of TIR imagery with a special interest in correction for atmospheric effects (cf. Refs. 12 through 14). This interest led to the development of SIG models, as described by Schott,⁶ incorporating bandpass values for transmission, up-welled and down-welled radiance, and angular emissivity effects. Although the SIG process used in these studies was primitive, it clearly demonstrated the need for inclusion of angular emissivity effects in TIRSIG. This work was extended by Schwartz et al.¹⁵ to include the effects of specular reflection of background surfaces and down-welled sky radiance. These scenes were still very "flat," with each scene segment treated

the same. This effect was addressed by Schott and Salvaggio,¹⁶ who describe incorporating brightness variations within segments by taking texture from images of laboratory physical models or from actual TIRSIG images. This was the first effort to make the TIRSIG images begin to look real. As part of these initial efforts to improve the "realism" of the SIG images, Schott and Salvaggio¹⁷ used a sensor response model incorporating image degradation using asymmetric two-dimensional convolution kernels to simulate atmospheric and optical detector sampling and scanning effects on the modulation transfer function of the imaging sensor. In addition, an ability to add random and periodic detector noise was developed and implemented. As the scenes became increasingly "real," the interest in simulation and its applications expanded. A full three-dimensional scene generation capability was achieved by incorporation of CAD/CAM three-dimensional wire frame models and a ray tracer as reported by Warnick et al.¹⁸ In parallel with these improvements, a series of small-scale validation efforts kept pace with the advances in SIG modeling, radiation propagation modeling, and materials measurement. The emissivity modeling was extended by Schott et al.¹⁹ to field measurements and to encompass the 3- to 5- μm and 8- to 14- μm regions with improved accuracies. Salvaggio and Schott²⁰ performed a validation study of the surface-leaving radiance portion of the model, validating the treatment of angular emissivity effects and the background and sky radiance equations used in the models. Shor et al.²¹ performed a preliminary validation of the radiometry and ray-tracing scheme used in conjunction with the 3-D wire frame modeling.

These studies affirmed the basic quantitative integrity of the methodology used but suggested the need for a variety of improvements. One of the most critical needs was for the incorporation of a thermal model so that temperatures could be predicted for each scene element, facet, or pixel based on object parameters and scene conditions. A second major improvement called for the inclusion of solar reflection effects. The modeling described above had been restricted to the LWIR bandpass where solar reflection and scattering effects are vanishingly small compared to self-emission. In the midwave region and at shorter wavelengths, solar reflection becomes very important and must be included in the SIG process. Spector et al.²² performed a study that included validation of a thermodynamic model that could be used in the SIG process and appeared to be quite accurate for passive objects. Salvaggio et al.²³ completed a study aimed at generation of spectral atmospheric radiation propagation and energy matter interaction terms needed for modeling solar and thermal radiometric effects associated with horizontal surfaces. This model could be modified for use in the SIG process and could also potentially be used spectrally (i.e., on a wavelength-by-wavelength basis) to improve the quantitative accuracy of the process. This is particularly important in wavelength regions where the source, sensor, or atmospheric spectral response is not spectrally flat such as in the MWIR or near the ozone absorption line in the LWIR.

Based on the assessment of the state of the art as described above and the status of the work of the DIRS laboratory at RIT, it was decided to assemble an IR SIG capability with all the base line capability for end-to-end image generation. This model would take advantage of existing

approaches and software whenever practical and would emphasize the generation of quantitatively correct radiometric scenes. The objectives of the model were that it should

1. function in the MWIR and LWIR regions
2. emphasize radiometry—in terms of dealing with as much radiometric phenomenology as necessary to reproduce observed phenomena
3. be capable of dealing with scene elements that would be observed by high-resolution airborne systems
4. use first principles physical models as much as possible
5. use simple target and sensor models in the initial versions to permit greater emphasis on the thermal and radiometric phenomenology (i.e., the objects are passive and have relatively few facets; sensor noise and jitter, which can be added in postprocessing, are not emphasized).

3 Scene Generation Approach

The DIRSIG model is comprised of several submodels. Each of the submodels is described in terms of its functionality and its primary interconnections with other submodels. This treatment is intended to provide the reader with an end-to-end view of the process. Since most of the submodels used are treated in detail elsewhere, only the interconnections are covered here along with the radiometry equations that govern the DIRSIG process and those attributes of the ray tracer that provide the submodel interconnections.

The first part of most SIG processes is the scene geometry submodel, which allows creation and location of objects in the scene. The DIRSIG scene geometry submodel uses a commercially available CAD package²⁴ called AutoCAD. This front end allows the user to interactively build wire frame representations of objects (cf. Fig. 1). The DIRSIG scene geometry submodel also allows for the scaling and orientation of objects to form the scene. In addition to forming the structure of objects and backgrounds, it is also necessary to assign material parameters to each surface in the scene. The DIRSIG scene geometry submodel uses faceted elements each of which has assigned to it attributes that allow all necessary optical and thermodynamic properties of the facet to be accessed. As part of the scene geometry submodel, the geometry data is translated from AutoCAD and formatted into real-world coordinates suitable for input to the DIRSIG ray tracer submodel. This translation and formatting process computes the normal vector outward, the slope, and the azimuthal angle for each facet (cf. Fig. 2).

The output from the scene geometry submodel is a hierarchical tree-type data structure, containing facet location, facet geometry, and material attributes, that serves as input to the ray tracer submodel. The ray tracer submodel draws on and interconnects all the other submodels to build the final scene. To initiate building a scene, the sensor model must be accessed to obtain the sensor location, orientation, angular fields of view, and the number of pixels to produce in the x and y directions for the raw radiance image (cf. Fig. 3). A ray is then traced through each pixel center into the scene, as shown in Fig. 4. The ray tracer uses a search process to determine which object, which part, and eventually which facet is hit. The hierarchical data structure and the use of bounding volumes around objects and parts fa-

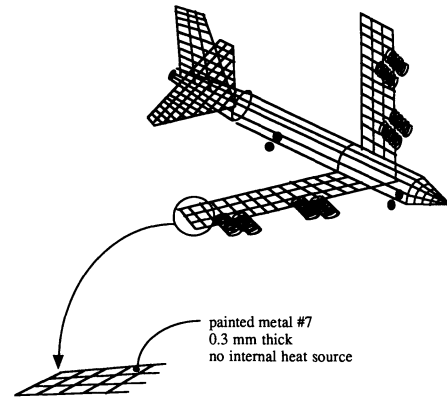


Fig. 1 Use of CAD routines to create three-dimensional, faceted wire frames containing individual facet property data.

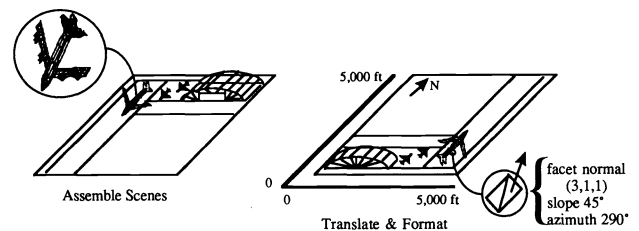


Fig. 2 Creation/assembly procedures accounted for by the scene geometry submodel.

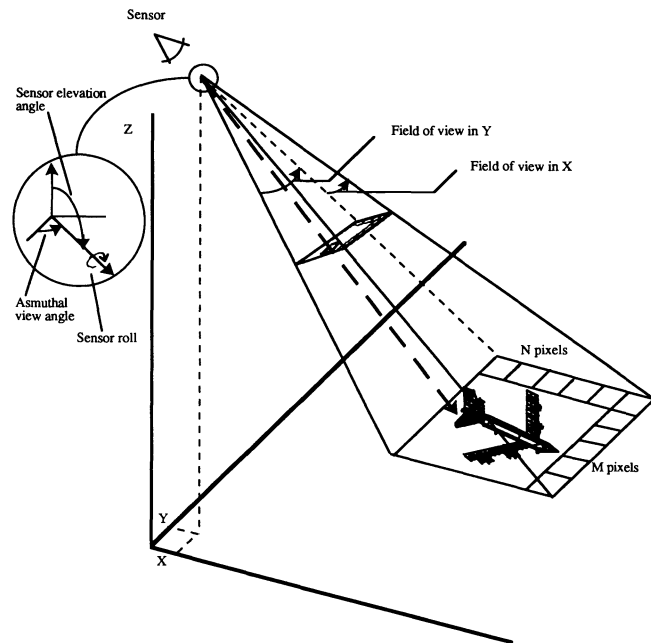
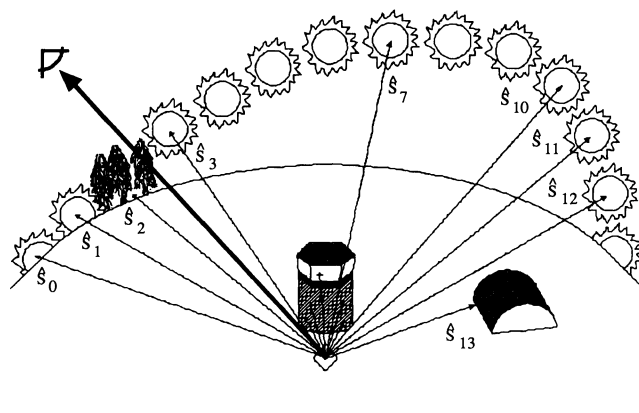


Fig. 3 How sensor geometry and field-of-view characteristics are used in the ray tracer.

Facilitate the search process. When a ray-facet intersection is located, a series of computations takes place to generate inputs to other submodels.

We first consider the data that are necessary to run the thermal submodel. The facet already has associated with it slope, azimuth, and material properties needed for thermodynamic and solar absorption computations. The material properties associated with each facet include solar absorp-



Sun/Shadow History Field

1	1	1	0	1	0	0	0	1	0	0	1	1	1	0	0	0
0	1	2	3	4	5	6	7	8	9	1	1	1	1	1	1	1
										0	1	2	3	4	5	

1 = Sun
0 = Shadow

Fig. 4 How a ray traced into the scene identifies a pixel center and how rays are cast out from that pixel center to identify sun shadow history.

tivity, broadband thermal emissivity, thickness, internal heat load, heat capacity, thermal conductivity, exposed area, specularity, and emissivity as a function of view angle and wavelength (if available). The major pixel specific unknowns are the current solar load and the solar history of the pixel. These data are acquired by the ray tracer casting out rays from the intersection point on the facet in the direction where the sun was at each point in time (e.g., from the time of the image and on $\frac{1}{2}$ -h intervals for the previous 24 h). The ray tracer determines if an object is hit or not and, therefore, if the pixel was sunlit or not, as shown in Fig. 4. This information is then submitted to the thermal model to compute the temperature of the individual pixel. The sun location information is computed from the time of day, latitude and longitude of the scene, and the day of the year, which are part of the overall scene data structure.

The thermal submodel²⁵ is built around THERM,²⁵ a temperature generation model, which provides most of its functionality. THERM can either use temporal meteorological data or compute estimates of the necessary data using simple environmental models. These meteorological data are combined with pixel specific material data and solar history and input to the thermal submodel, which solves the linear differential heat flow equation for the temperature of the pixel. Figure 5 illustrates some of the variables accounted for in the thermal submodel. THERM's relative ease of implementation, coupled with the fact that it is one of the few thermal models of naturally occurring surfaces that has any degree of validation, made it attractive for use as the thermodynamic model.

The temperature of any pixel is a function of the thermodynamic properties of the facet as well as the environmental history to which it has been exposed. THERM was designed to compute the temperature of facets (assuming no lateral conduction) by combining facet specific parameters (heat capacity, thermal conductivity, thickness, solar absorptivity, exposed area, self-generated power, and slope and azimuth angles) with time-dependent environmental parameters (direct insolation, diffuse insolation, air temper-

ature, wind exposure, cloud type, speed, air pressure, relative humidity, sky temperature, precipitation type, and rate). Each computation is initiated with an equilibrium solution at some previous point in time, and then the current temperature is solved for using a series of forward chaining solutions to the heat flow equations. For objects with high thermal inertia, it was found necessary to initiate the process as much as 24 h ahead of the actual simulation time. THERM is designed to accept either measured environmental data or to approximate time-dependent environmental data from standard forecast data or weather records. Because solar insolation is such a driving factor in temperature computations, THERM was modified for inclusion in DIRSIG. This modification allowed pixel specific computation of temperature by determining whether the pixel was sunlit at the time of interest and what the shadow history of the pixel had been. These data are then used to modify the temporal insolation data on a pixel specific basis. This was accomplished by a simple modification to the magnitude of the solar insolation value used in the THERM computations. These temporal values are set equal to zero for any time when the pixel would have been in shadow. This capability is essential if realistic computations in the vicinity of shadowing objects is required.

Spector et al.²² have shown that THERM produces accurate temporal predictions of temperatures of passive real-world objects. Figure 6 shows actual object temperatures compared to THERM predicted object temperatures. THERM does not compute the conduction between adjacent object facets and therefore does not have all of the functionality of a fully conducting model, which would require the use of finite element analysis. Such models are complex and require substantial amounts of computing time to add facet-to-facet conduction. THERM does allow for facets with self-generated (internal) power that can, when properly implemented, be used to overcome some of the limitations of nonconduction between facets.

Having received the temperature of the pixel from the thermal submodel, the ray tracer generates additional pixel specific data needed for the radiometry submodel. These include computation of the interaction angles between the incident solar ray and the normal to the facet, the angle between the normal to the facet and the ray from the sensor, the angle between the normal to the earth and the sensor, and the direction of specular reflection if the object is specular. The specular ray is projected to determine whether the sky or a background object is encountered. If a background object is hit, additional data is gathered using the ray tracer and the thermal submodel for the background (cf. Fig. 7). The model currently assumes each material is either perfectly diffuse or perfectly specular with the magnitude of the specular reflection a function of look angle. If no object is hit, then the radiance from the particular location in the sky is computed.

The angular data, target temperature, background data, etc. are then passed to the radiometry submodel, which computes the radiance reaching the sensor on a wavelength-by-wavelength basis. Figure 8 shows some of the energy paths and energy matter interactions included in the radiometry submodel. The radiometry submodel is built on top of LOWTRAN 7. The atmospheric transmission, up-welled radiance, solar irradiance, and down-welled radiance are

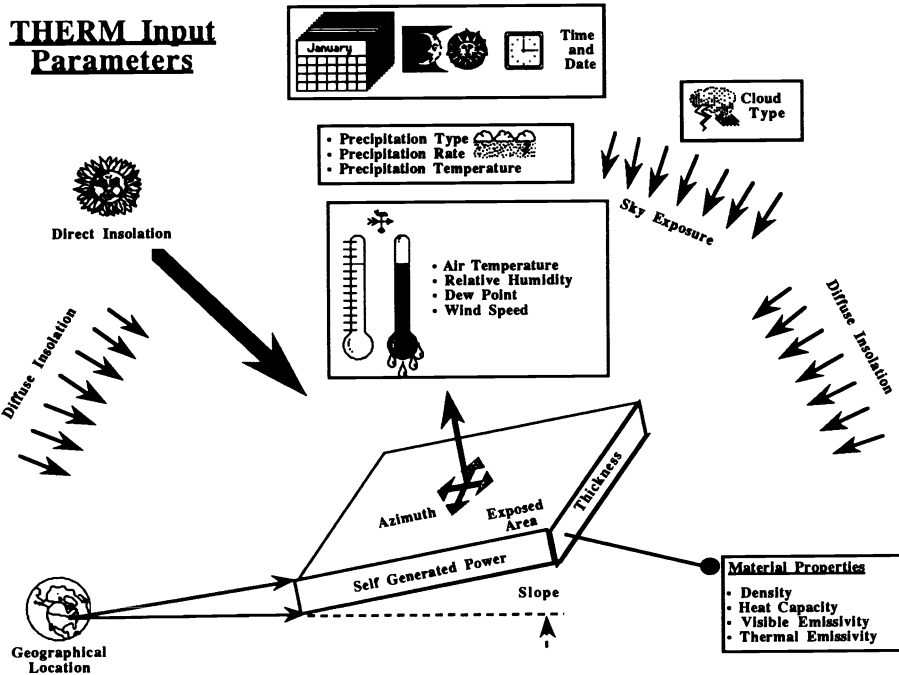


Fig. 5 Some of the variables accounted for by the thermal submodel.

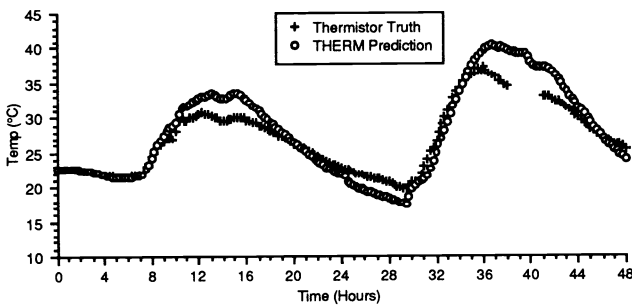


Fig. 6 Actual object temperature (thermistor truth) versus THERM predicted temperature as a function of time.²²

precomputed for each wavelength within the spectral band of interest and for the range of possible slant paths within the scene (cf. Fig. 9). The appropriate radiometry equation is then solved and numerically integrated over wavelength using the spectral response function of the sensor as a weighting factor to yield the effective integrated radiance at the sensor for each pixel.

Each pixel falls into one of four categories (cf. Fig. 10) and is processed through the appropriate governing equation. For pixels having diffuse reflectance characteristics (case 1), the radiance is

$$\begin{aligned}
 L(\theta, \lambda) = & \epsilon(0, \lambda) L_T(\lambda) \tau_2(\theta_E, \lambda) \\
 & + I_T \frac{E_S(\lambda)}{\pi} \tau_1(\lambda) \cos(\theta_S) [1 - \epsilon(0, \lambda)] \tau_2(\theta_E, \lambda) \\
 & + [L_{DE}(\lambda) + L_{DS}(\lambda)] [1 - \epsilon(0, \lambda)] \tau_2(\theta_E, \lambda) \\
 & + L_{UE}(\theta_E, \lambda) + L_{US}(\theta_E, \lambda) .
 \end{aligned} \tag{1}$$

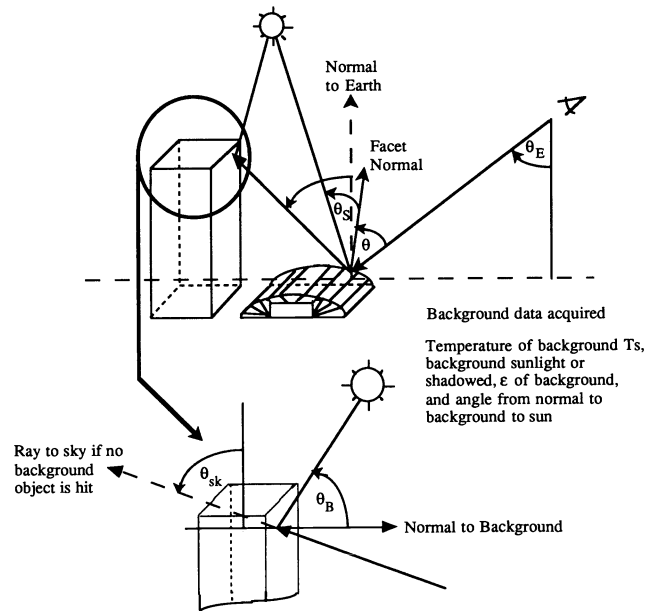


Fig. 7 Ray interaction with a specularly reflecting surface.

For pixels having specular reflectance characteristics, where the reflected ray bounces to the sky (case 2), the radiance is

$$\begin{aligned}
 L(\theta, \lambda) = & \epsilon(\theta, \lambda) L_T(\lambda) \tau_2(\theta_E, \lambda) \\
 & + I_T \frac{E_S(\lambda)}{\pi} \tau_1(\lambda) \cos(\theta_S) [1 - \epsilon(\theta, \lambda)] \tau_2(\theta_E, \lambda) \\
 & + [L_{DE}(\theta_{SK}, \lambda) + L_{DS}(\theta_{SK}, \lambda)] [1 - \epsilon(\theta, \lambda)] \tau_2(\theta_E, \lambda) \\
 & + L_{UE}(\theta_E, \lambda) + L_{US}(\theta_E, \lambda) .
 \end{aligned} \tag{2}$$

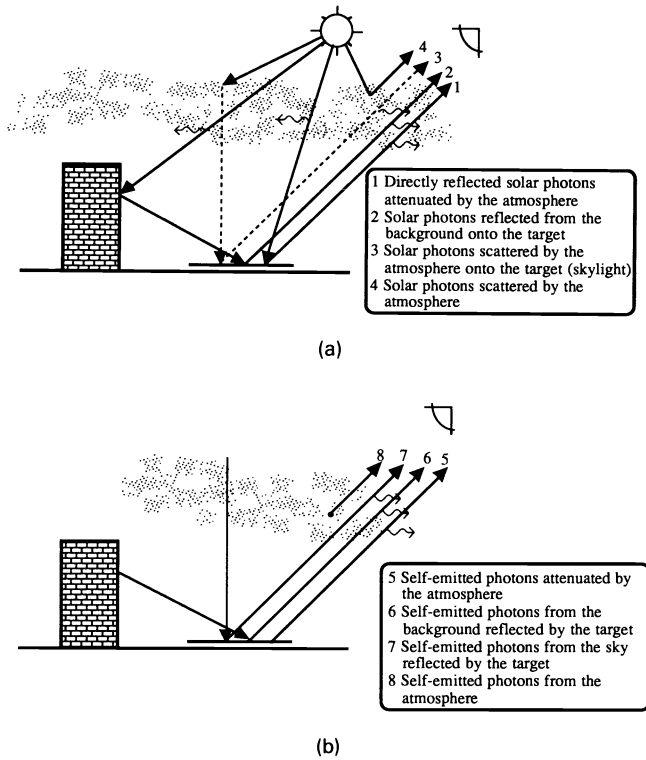


Fig. 8 (a) Some of the solar energy paths included on a wavelength-by-wavelength basis by the radiometry submodel; (b) some of the self-emitted energy paths included on a wavelength-by-wavelength basis by the radiometry submodel.

For pixels having specular reflectance characteristics, where the reflected ray hits a background object (case 3), the radiance is

$$\begin{aligned}
 L(\theta, \lambda) = & \varepsilon(\theta, \lambda)L_T(\lambda)\tau_2(\theta_E, \lambda) \\
 & + I_T \frac{E_S(\lambda)}{\pi} \tau_1(\lambda) \cos(\theta_S)[1 - \varepsilon(\theta, \lambda)]\tau_2(\theta_E, \lambda) \\
 & + \varepsilon_B(\theta_{BT}, \lambda)L_{TB}(\lambda)[1 - \varepsilon(\theta, \lambda)]\tau_2(\theta_E, \lambda) + I_B \frac{E_S(\lambda)}{\pi} \tau_1(\lambda) \\
 & \times \cos(\theta_B)[1 - \varepsilon_B(\theta_{BT}, \lambda)][1 - \varepsilon(\theta, \lambda)]\tau_2(\theta_E, \lambda) \\
 & + L_{UE}(\theta_E, \lambda) + L_{US}(\theta_E, \lambda) .
 \end{aligned} \quad (3)$$

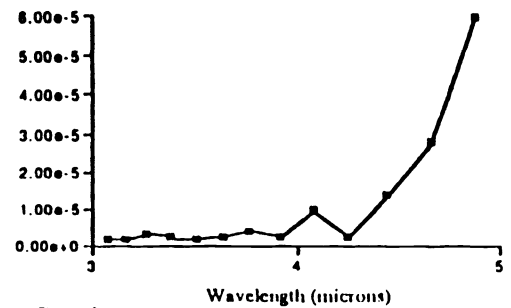
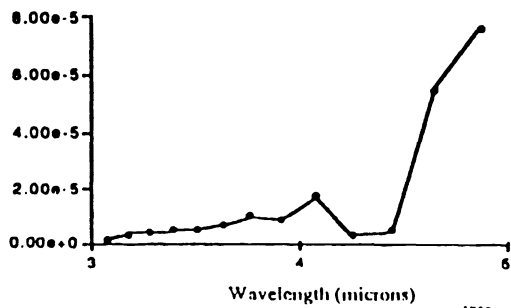
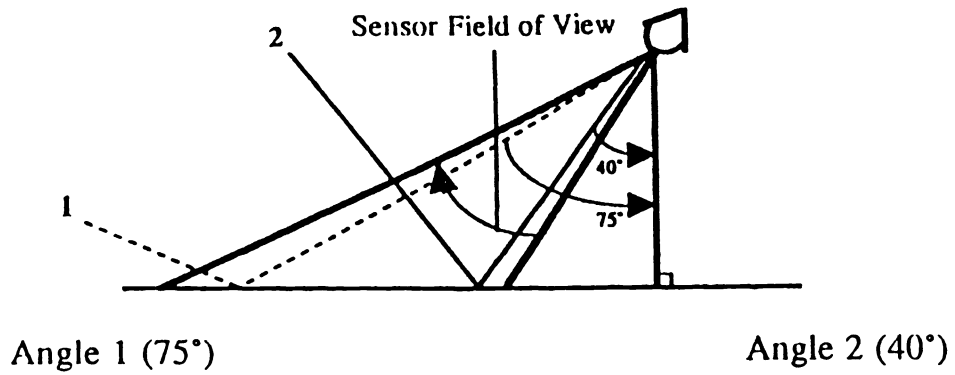
Finally, for pixels where a ray cast from the sensor heads to the sky (case 4), the radiance is

$$L(\theta, \lambda) = L_{DE}(\theta_{SK}, \lambda) + L_{DS}(\theta_{SK}, \lambda) . \quad (4)$$

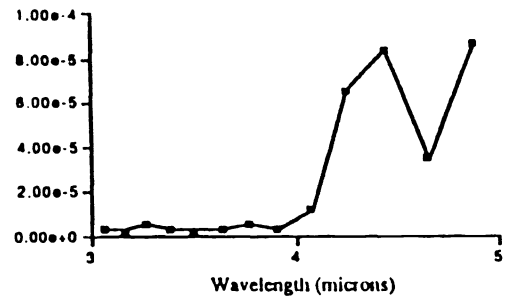
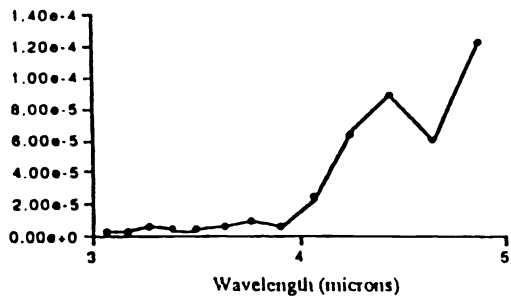
The parameters in Eqs. (1) through (4) are defined below. It is important to realize that wherever a functional dependence on an angle (e.g., θ, θ_{SK}) is indicated, an array of values are precomputed and the actual value solved by interpolation. All parameters with a functional dependence on wavelength (λ) are generated on 100-cm^{-1} intervals over the range 350 to 39850 cm^{-1} (0.25 to $28\text{ }\mu\text{m}$). (Improvements are underway to eliminate the current 100-cm^{-1} spectral resolution limitations.)

- $L(\theta, \lambda)$ = spectral radiance reaching the front end of the sensor
- $L_T(\lambda)$ = the self-emitted spectral radiance from a blackbody at temperature T (target)
- $L_{TB}(\lambda)$ = the self-emitted spectral radiance from a blackbody at temperature T (background)
- $E_S(\lambda)/\pi$ = the exoatmospheric solar spectral radiance
- $L_{DE}(\lambda)$ = the down-welled spectral radiance due to self-emission of the atmosphere integrated over the skydome
- $L_{DS}(\lambda)$ = the down-welled spectral radiance due to scattering integrated over the skydome
- $L_{DE}(\theta_{SK}, \lambda)$ = the directional down-welled spectral radiance due to self-emission of the atmosphere
- $L_{DS}(\theta_{SK}, \lambda)$ = the directional down-welled spectral radiance due to solar scattering
- $L_{UE}(\theta, \lambda)$ = the up-welled spectral radiance due to self-emission of the atmosphere along the target-sensor path
- $L_{US}(\theta, \lambda)$ = the up-welled spectral radiance due to solar scattering along the target-sensor path
- $\tau_1(\lambda)$ = the atmospheric spectral transmission along the sun-target path
- $\tau_2(\theta_E, \lambda)$ = the atmospheric spectral transmission along the target-sensor path
- $\varepsilon(\theta, \lambda)$ = angular spectral emissivity for the target
- $\varepsilon_B(\theta, \lambda)$ = angular spectral emissivity for the background
- θ = the angle between the normal to the surface and the sensor-target path
- θ_S = the angle between the normal to the surface and the sun-target path
- θ_B = the angle between the normal to the background and the sun-background path
- θ_E = the angle between the normal to the earth at the target and the sensor-target path
- θ_{SK} = the angle between the normal to the earth and the ray reflected specularly from the sensor at the target
- θ_{BT} = the angle between the normal to the background and the target hit point
- I_T = target sun/shadow flag (1 or 0) (indicates presence or absence of shadow)
- I_B = background sun/shadow flag (1 or 0) (indicates presence or absence of shadow).

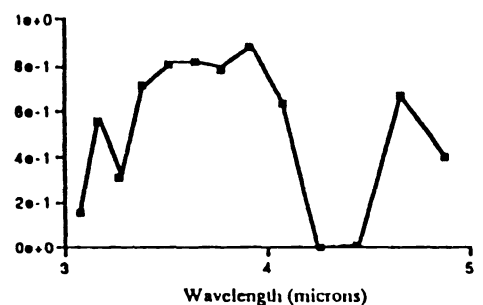
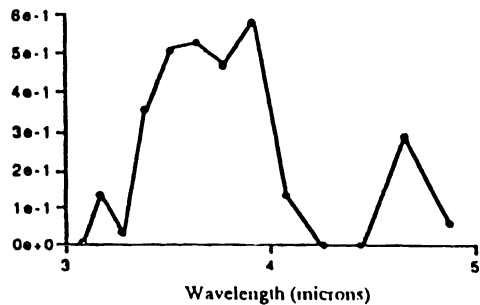
These parameters are defined using the preceding submodels and a modified version of LOWTRAN 7 that produces output tables of the standard LOWTRAN radiometric terms as a function of wavelength. Additional terms are generated by manipulation of the basic LOWTRAN code (e.g., numerical integration of paths to space to yield down-welled sky radiance). The LOWTRAN-derived values can



Thermal Upwelled Radiance
TLU



Thermal Downwelled Radiance
TLD



Atmospheric Transmission
TAU 2

Fig. 9 How radiometric terms vary with both view angle and wavelength.

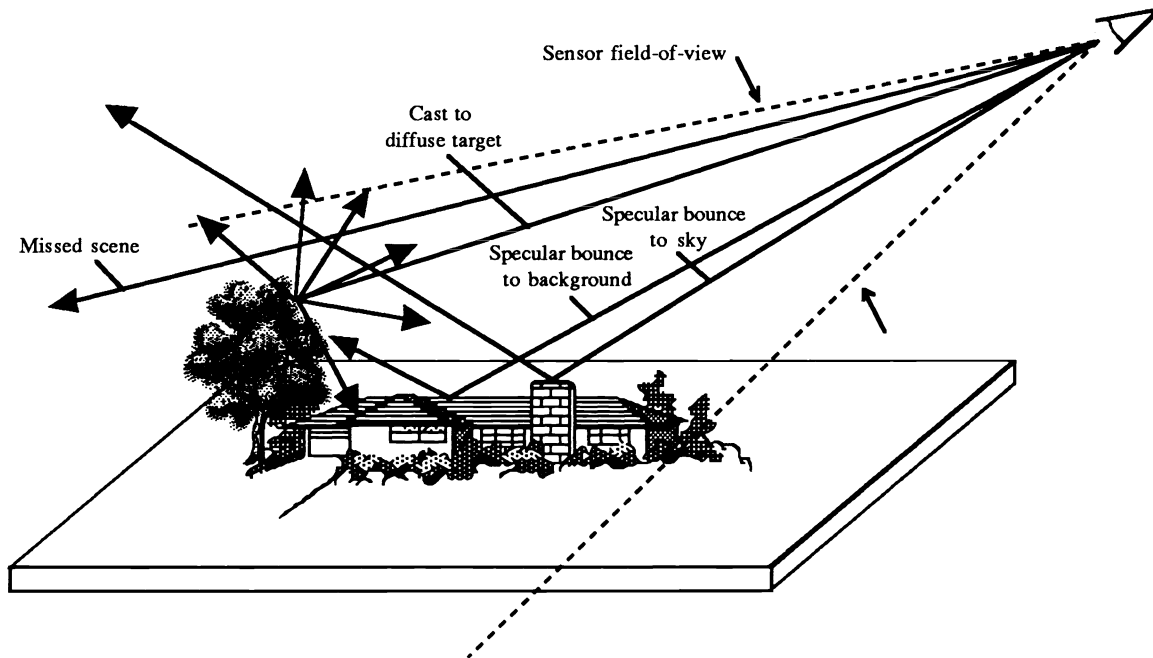


Fig. 10 Possible ray interactions on a target within the scene.

be derived from user-supplied atmospheric profile (radiosonde) data or using the standard atmospheres found in LOWTRAN.

After each pixel's radiance has been computed, the composite radiance image can be passed to a sensor model, such as described by Schott and Salvaggio.¹⁶ This model allows for geometric corrections to a radiance image to account for blurring by the atmosphere, optics, sensor motion, and electronics as well as for sampling effects of the detector and electronics. This type of sensor submodel can also add random and periodic noise effects. Schott and Salvaggio¹⁷ describe how it is also possible to add random or periodic texture within an object class to simulate variations in optical or thermal properties within the material type. For the images presented here, texture variations and degradations due to the sensor are not included except for radiometric quantization. Figure 11 shows a flow diagram of how the various models are interconnected.

4 Results

The results of phenomenological testing of the model are presented here. The intent was to exercise several aspects of the model and determine if phenomena normally observed in midwave infrared and longwave infrared images could be simulated. A major test of the model was to determine how well it would model variations in the appearance of a scene as a function of time. Figure 12 shows eight frames from a 24-h sequence simulating parked aircraft. The images show the scene from 8 a.m. to 3 p.m. as simulated in the 3- to 5- μm bandpass.

The effects of the differential thermal mass of the runways, parking apron, grass, and aircraft are clearly simulated with high thermal mass objects heating up more slowly and staying warm longer. The shadows move about the scene as expected (note the planes are facing north). In particular, note the separation into a sharp and a blurred shadow cast by the nose of the large aircraft in the early

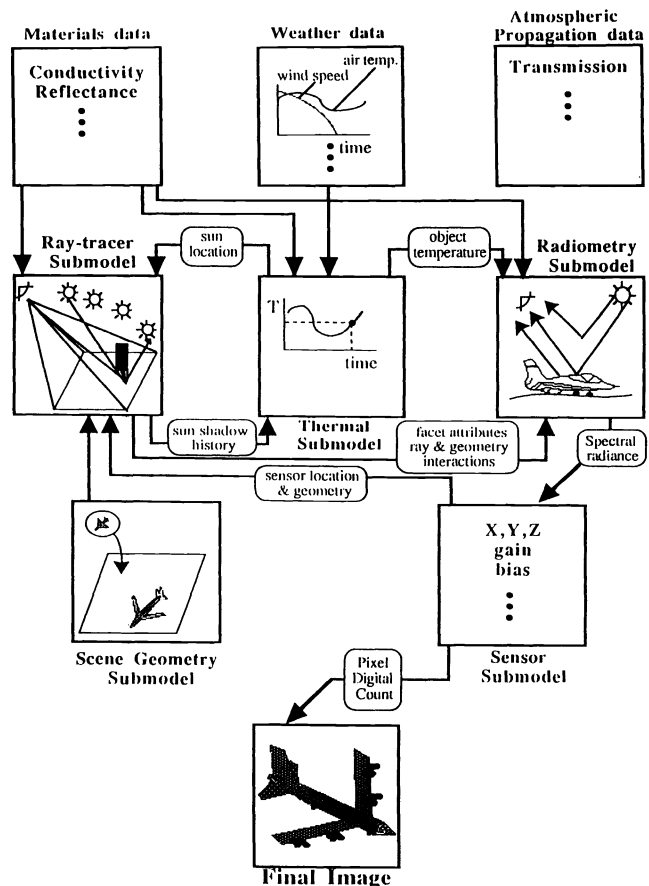


Fig. 11 Interactions between submodels in the DIRSIG model.

afternoon. In this region of the spectrum, the photon flux from reflected solar photons is of the same order of magnitude as from self-emitted (thermal) photons. The sharp shadow is formed when the sun is blocked. The blurred shadow is caused because the region to the west of the

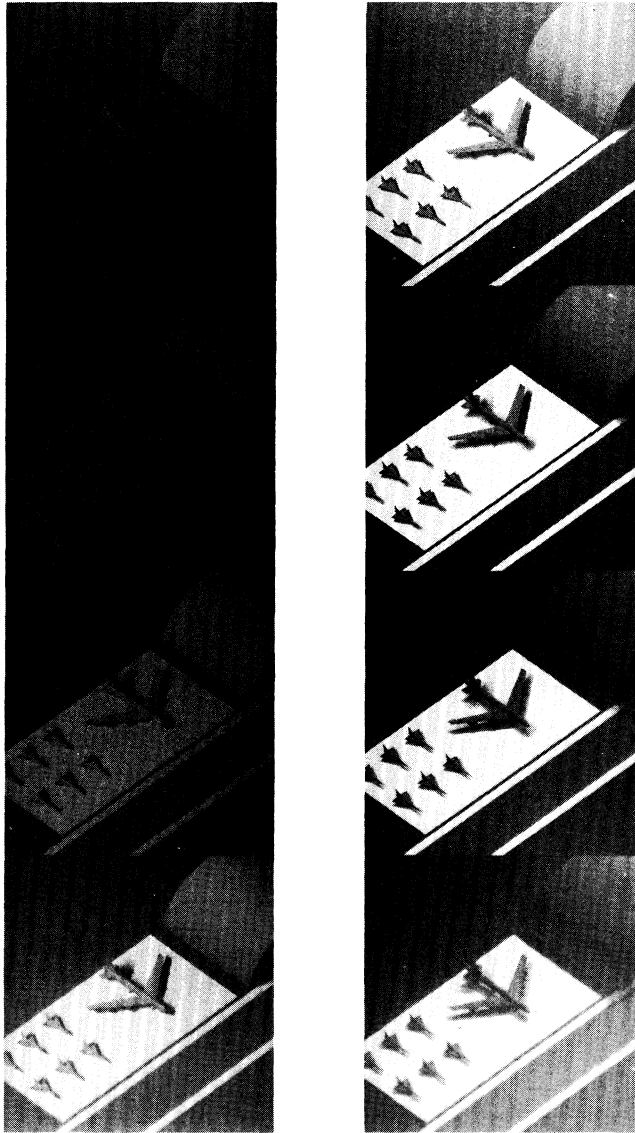


Fig. 12 Simulated images in the 3- to 5- μm bandpass. These images simulate how the scene would appear at 8, 9, 10, and 11 a.m. (left column) and 12 noon, 1, 2, and 3 p.m. (right column).

current shadow was previously in shadow and is therefore cooler and radiating fewer photons. A similar image sequence in the 8- to 14- μm region shows only the thermal shadow. Again, this is an expected result because very few solar photons are observed in the 8- to 14- μm window.

The variation in brightness across the surface of the hangar and the aircraft fuselage also simulate observed phenomena caused by differential heating due to the angle between the surface normal and the sun in addition to variations in emissivity associated with differences between the surface normal and view angle.

The DIRSIG model's capability for simulating weather conditions on thermal infrared images is shown in Fig. 13. This sequence of images illustrates the effect of various wind flow conditions. These images simulate how the wind speed has a significant impact on reducing the contrast in thermal images. The images are simulated as though the wind had blown at a constant speed of 0, 10, 20, or 30 mph

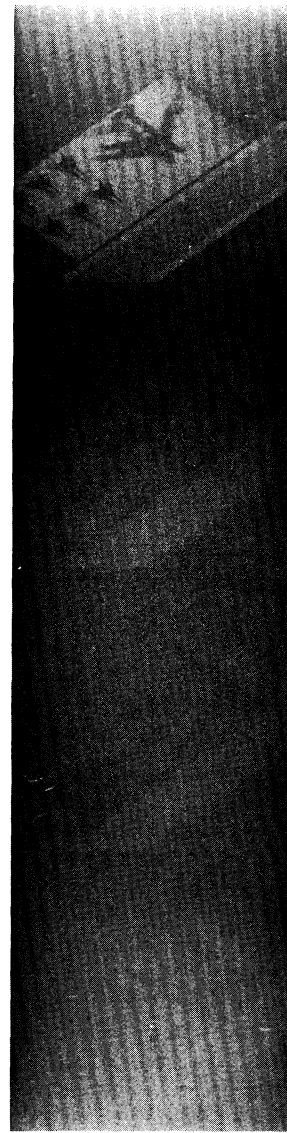


Fig. 13 Simulated images in the 8- to 14- μm bandpass. These images show how the scene would vary if the wind speed changed. They were modeled with fixed wind speeds of 0, 10, 20, and 30 mph (top to bottom) for the previous 24 h.

for the 24 h preceding the time of image simulation. This shows a well-known phenomena of contrast reduction associated with wind speed and the nonlinearity of this process (i.e., rapid contrast reduction and then only more gradual contrast reduction at higher wind speeds). The effects of the atmosphere and view angle variations are illustrated in Fig. 14. These images represent a series of acquisitions at a fixed range of 10 km at a series of view angles in the 8- to 14- μm bandpass. The optical depth at the more grazing angles is much deeper than at near vertical views, resulting in reduced contrast with the angle. Also shown in these images is the effect of varying emissivity as a function of view angle. This is most dramatic at the lowest (most grazing) view angle where the top of the hangar becomes very dark (cold). At grazing angles, the reflectivity of specular materials (such as the painted metal hangar roof) becomes nearly mirrorlike. This results in a specular glint to a "cold" sky. These synthetic images mimic the phenomena that are

observed in actual imagery. In general, the synthetic images generated by the model produce to first order most of the thermal, atmospheric, and optical phenomena observed by the thermal infrared sensors. Because the ray tracer can be run at any resolution supported by the object models; aliasing effects, inherent in ray tracers, can be minimized by producing radiance scenes with higher resolution than required and convolving with a kernel simulating the point spread function of the sensor.

The results presented above do not provide information as to how well the model performs in a quantitative fashion. Many aspects of the submodels have of course been quantitatively evaluated. Spector et al.²² describes a limited evaluation of the thermal model indicating that for passive objects it tracks temperature to better than 1.5 K when good meteorological data are available. Several aspects of LOW-TRAN's performance have been documented (cf. Ref. 2). The angular emissivity and surface-leaving radiance components of the model were tested by Salvaggio and Schott,¹⁶ and the link to a ray tracer was further tested by Shor et al.²¹ These data indicate that earlier versions of the optical interactions and ray tracer would be expected to yield sensed radiance values within 2 K of the actual values when the surface temperatures are known. These peripheral tests tend to add credence to the overall model, however, future efforts should address their quantitative accuracy.

5 Conclusions and Recommendations

The synthetic image generation model described here exhibits a wide range of capabilities. The model starts with three-dimensional geometric objects each with sets of physical descriptors, assembles these individual objects into a faceted scene, assigns temperatures to each facet in the objects based on a thermodynamic model, uses ray tracing techniques to determine the radiometric interaction that occurs at each point in the scene, computes the radiance reaching the front end of a sensing system, models the sensor used to record the signal, and produces a realistic synthetic image in the LWIR or MWIR bandpass.

Finally, the results presented here represent a proof-of-concept demonstration of an engineering model so that no run-time performance test has been made, nor has any attempt been made to optimize the run time of the code. The run time is very much a function of the complexity of the scenes (number of objects and number of facets per object), the number of pixels in the scene, number of spectral intervals in the bandpass, the time interval for thermal history computations, and the number of hours of thermal history required for temperature calculations. For the scenes presented here there were 24 objects consisting of a total of 4772 facets. The thermal model was run on 15-min increments (shadow location updated on 30-min increments) for the 24 h prior to image creation time. The 512×512 scenes presented here had run times of approximately 15 h on a VAX 4000 Model 300. As indicated above, no effort has been placed into optimizing this code. We believe that substantial improvements in serial processing speed can be obtained and the process is very amenable to parallel processing.

The images produced depict most of the phenomena that one would expect to see in real imagery with proper radiometric fidelity and geometric interactions. This tool enables scientists, engineers, and analysts to visualize the scenes



Fig. 14 Simulated images in the 8- to 14- μm bandpass. These images show how the scene would appear when viewed from a fixed slant range at angles from the vertical of 0, 15, 30, 45, 60, and 75 deg.

that can be produced by a sensor of interest under a variety of meteorological and collection geometry conditions. The "what if" research that can be conducted with such a tool and the educational potential for image analysts are nearly unlimited.

Although the model appropriately mimics much of thermal imaging phenomena, several weaknesses remain. Its overall quantitative accuracy needs to be tested and the limitations of each of the submodels identified. The thermal model is quite effective in dealing with environmental influences, however, it does not account for internal conduction and lateral dispersion of energy from internal heat sources such as automobile engines. Future efforts should consider using a heat-flow model incorporating internal conduction effects or a hybrid model that merges the current model with an internally conducting model. The radiometry model described here is limited in that objects are treated as either completely diffuse or completely specular. The potential for fully incorporating bidirectional reflectance factors (BRDF) should be considered. If this were to be fully implemented, the effects of background objects on both the thermodynamic and radiometric models could be more accurately modeled. This improvement in the accuracy might, however, be expensive in terms of computing time, therefore, enhancements that don't involve full BRDF but that reduce the current limitations should also be considered. Finally,

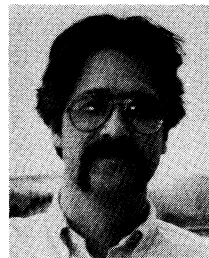
for uses where spatial variation within a material class is important, improved methods for modeling and incorporating texture into TIRSIG images should be studied.

Acknowledgments

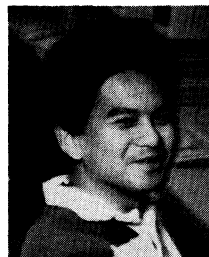
The authors are grateful for the support of the research staff and students in the DIRS lab who have contributed to the programs that have led up to this work, to C. Kitchen for her diligence in assembling this manuscript, and to the reviewers for their thoughtful review and encouragement.

References

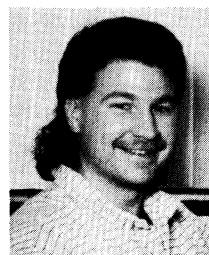
- DCS Corporation and J. R. Schott, "Automatic target recognition/counter-countermeasures technology development program model review," DCS Report No. 13430LT003Z, Autometric Incorporated (1987).
- F. X. Kneizys, E. P. Shettle, L. W. Abreu, J. H. Chetwynd, G. P. Anderson, W. O. Gallery, J. E. A. Selby, and S. A. Clough, "Users guide to LOWTRAN 7, AFGL-TR-88-0177," Environmental Research Paper No. 1010, Air Force Geophysics Laboratory, Optical/Infrared Technology Division, Hanscom AFB, Maryland (1988).
- J. M. Cathcart and A. D. Sheffer, "Target and background infrared signature modeling for complex synthetic scenes," in *Infrared Systems and Components II*, H. M. Liaw, Ed., *Proc. SPIE* **890**, 95-103 (1988).
- A. D. Sheffer and J. M. Cathcart, "Computer generated IR imagery: a first principles modeling approach," *Proc. SPIE* **933**, 199-206 (1988).
- E. Botkin, G. Kelley, and G. Gawronski, "Infrared modeling and analyses (IRMA)," Report AFATL-TR-81-65, Grumman Aerospace Corporation, Bethpage, N.Y. (1981).
- J. R. Schott, "Incorporation of angular emissivity effects in longwave infrared image models," in *Infrared Technology XII, Proc. SPIE* **685**, 44-52 (1986).
- J. M. Cathcart and A. D. Sheffer, "Generation and application of high-resolution infrared computer imagery," *Opt. Eng.* **30**(11), 1745-1755 (1991).
- H. Biesel and T. Rohlfing, "Real-time simulated forward looking infrared (FLIR) imagery for training," in *Infrared Image Processing and Enhancement*, M. R. Weathersby, Ed., *Proc. SPIE* **781**, 71-80 (1987).
- G. H. Kornfeld, "Digital simulation of precise sensor degradations including nonlinearities and shift variance," in *Infrared Image Processing and Enhancement*, M. R. Weathersby, Ed., *Proc. SPIE* **781**, 63-70 (1987).
- G. Y. Gardner, J. Mendelsohn, J. Kim, and W. Reynolds, "A digital scene model for simulation of visual and infrared imagery," in *Infrared Image Processing and Enhancement*, M. R. Weathersby, Ed., *Proc. SPIE* **781**, 81-86 (1987).
- J. Stets, J. Conant, J. Gruninger, and B. Ryali, "Synthetic IR scene generation," in *Infrared Systems and Components II*, H. M. Liaw, Ed., *Proc. SPIE* **890**, 130-146 (1988).
- J. R. Schott and E. W. Schimming, "Data use investigations for applications explorer mission A (heat capacity mapping mission)," Calspan Report No. 6175-M-1, NASA Accession #E81-10079 (Jan. 1981).
- J. R. Schott and W. J. Volchok, "Thematic mapper thermal infrared calibration," *Photogrammetric Eng. Remote Sensing* **51**(9), 1351-1357 (1985).
- A. E. Byrnes and J. R. Schott, "Correction of thermal imagery for atmospheric effects using aircraft measurement and atmospheric modeling techniques," *J. Appl. Opt.* **25**(15), 2563-2570 (1986).
- I. B. Schwartz, K. A. Snail, and J. R. Schott, "Infrared halo effects around ships," Naval Research Laboratory Memorandum 5529 (1985).
- J. R. Schott and C. Salvaggio, "LWIR radiometric modeling for use with synthetic scene generation 1987/88 results," Final Report RIT/DIRS 87/88-51-122, prepared for Contract RD-86-6843 (Task 3), Office of Development and Engineering, Central Intelligence Agency (Jan. 1989).
- J. R. Schott and C. Salvaggio, "Inclusion of sensor noise in radiometric models for generation of synthetic longwave infrared images," in *Three-Dimensional Imaging and Remote Sensing, Proc. SPIE* **819**, 42-54 (1987).
- J. S. Warnick, E. Shor, and J. R. Schott, "Thermal infrared scene simulation," Final Report RIT/DIRS 89/90-51-133, United States Department of Energy (Jan. 1990).
- J. R. Schott, M. Fairchild, X. Feng, R. Raqueno, B. Brower, and T. Gallagher, "Techniques for measurement of the optical properties of materials," Final Report RIT/DIRS 89/90-51-134, United States Department of Energy (Jan. 1990).
- C. Salvaggio and J. R. Schott, "Laboratory techniques for assessment of longwave infrared radiometric models for synthetic scene generation," in *Infrared Technology XV, Proc. SPIE* **1157**, 102-114 (1989).
- E. H. Shor, C. Salvaggio, and J. R. Schott, "Three-dimensional longwave infrared (LWIR) synthetic image generation incorporating angular emissivity effects using raytracing techniques," in *Infrared Technology XVI, Proc. SPIE* **1341**, 68-79 (1990).
- D. N. Spector, P. F. Lambeck, S. L. Sheller, S. C. Sawtell, D. K. Rankin, and J. R. Schott, "Air Force infrared simulated image models," ERIM Rept. #213400-53-X(II), *Proc. Infrared Information Symp.* **35**(2), 71-90 (1991).
- C. Salvaggio, G. Braun, and J. R. Schott, "SVGM a spectral vector generating model using the LOWTRAN 7 and SCATRAN atmospheric propagation codes," RIT/DIRS 90/91-63-141, Eastman Kodak Company, Federal Systems Division (Jan. 1991).
- Autocad Release 10 Reference Manual*, Autodesk Inc. (1989).
- DCS Corporation, "AIRSIM thermal signature prediction and analysis tool model assumptions and analytical foundations," DCS Technical Note 9090-002-001 (1991).



John R. Schott is a professor in the Center for Imaging Science at the Rochester Institute of Technology (RIT) and head of the Center's Digital Imaging and Remote Sensing Laboratory. Prior to joining RIT, Dr. Schott was a principal physicist with Calspan Corporation (1972-1980). He has a BS in physics/sociology from Canisius College and MS and PhD degrees in environmental engineering from SUNY Syracuse. He is a member of the SPIE, ASPRS, CRSS, and Sigma Xi. His research is focused on developing techniques to acquire and extract information from remotely sensed images. His interest in quantitative radiometric image analysis led to his serving as a principal investigator for NASA's Landsat 4/5 Thematic Mapper Program.



Rolando Raqueno received his BS in engineering and premedicine from the Mechanical Engineering Department at The Catholic University of America in 1985 and his MS in computer science from the Rochester Institute of Technology (RIT) in 1990. Between 1985 and 1990, he worked as a research assistant and then as an associate scientist/engineer with the Digital Imaging and Remote Sensing Laboratory in the Center for Imaging Science at RIT. His research involvement and interests at the center include development of image processing algorithms for medical imagery; multivariate and multispectral analysis of satellite data; and midwave and longwave infrared scene simulation, modeling, and measurement. He is currently a development engineer with the Federal Systems Division of Eastman Kodak and is also an adjunct faculty member with CIS. He is a member of Tau Beta Pi.



Carl Salvaggio is a research scientist in the Center for Imaging Science at the Rochester Institute of Technology. He received his BS and MS in imaging science from the Rochester Institute of Technology in 1987 and is working on his doctorate at SUNY College of Environmental Science and Forestry in Environmental Resource Engineering. His research activities include multispectral synthetic scene generation, atmospheric propagation models, scene normalization, image processing, and computer graphics. He is a member of the American Society for Photogrammetry and Remote Sensing and is president of the Central New York Region of ASPRS.